Supporting Information for

Ion Selective Covalent Organic Framework Enabling Enhanced Electrochemical Performance of Lithium-Sulfur Batteries

Yu Cao, Hong Wu, Gang Li, Cheng Liu, Li Cao, Yiming Zhang, Wei Bao, Huili Wang, Yuan Yao, Shuo Liu, Fusheng Pan, Zhongyi Jiang,* and Jie Sun**

*Corresponding author. E-mail: fspan@tju.edu.cn; zhyjiang@tju.edu.cn; jies@tju.edu.cn.

Experimental Procedures

Preparation of TpPa-SO_3H Nanosheets

TpPa-SO_3H nanosheets were prepared through an interfacial polymerization method according to the reported literature.[1] 21 mg of 1,3,5-Triformylphloroglucinol was dissolved in 20 mL n-octanoic acid as the upper organic phase, and 28.2 mg 2,5-diaminobenzenesulfonic acid was dissolved in 30 mL deionized water as the lower aqueous phase. The interfacial reaction was kept at 17 ^oC for 72 h, and the TpPa-SO_3H nanosheets was produced in the interface and sank in the aqueous phase. Dialysis method was used to remove the impurity in the abundant deionized water for 72 h. The concentration of final TpPa-SO_3H nanosheets dispersion was around 0.8 mg mL^{-1}.

Preparation of TpPa-SO_3Li Nanosheets

A chemical lithiation method was used to prepare TpPa-SO_3Li Nanosheets. 10 g lithium acetate was added into the 30 mL TpPa-SO_3H nanosheets aqueous dispersions, and the suspension was stirred at 60 ^oC for 72 h. Dialysis was conducted for removing uncoupled lithium-ion using deionized water for 24 h. The concentration of final TpPa-SO_3Li dispersion was around 0.15 mg mL^{-1}.

Preparation of TpPa-SO_3Li/Celgard Separator

The TpPa-SO_3Li/Celgard Separators were fabricated by depositing TpPa-SO_3Li nanosheets onto one side of the commercial Celgard separator through a vacuum-assisted self-assembly method. 5 mL TpPa-SO_3Li dispersion were added into 20

mL ethanol solution and ultrasonicated for 30 min to form a very homogeneous dispersion. Then the suspension of the TpPa-SO_3Li nanosheets was deposited onto the Celgard separator via vacuum filtration. The diameter of TpPa-SO_3Li/Celgard Separator is 16 mm, and the mass loading was approximately 0.37 mg cm^{-2}. The TpPa-SO_3H/Celgard Separators were also fabricated as the control samples using the same method.

Preparation of CNT Interlayer

CNT was dispersed in the ethanol solution. Then the suspension of CNT was filtrated onto the Celgard separator. After drying, a self-supporting CNT interlayer was obtained, and the mass is around 1.0 mg with a diameter of 16 mm. The CNT is a free-standing interlayer between the S cathode and TpPa-SO_3Li/Celgard separator.

Materials Characterization

The FTIR spectra was recorded on a BRUKER Vertex 70 equipment. ICP-OES was done on an Agilent 720-ES with a CCD-detector. TEM images and element distribution mappings were collected by a JEM-2100F instrument. AFM images were taken by Bruker Dimension icon. SEM images and element distribution mappings were observed by Hitachi S-4800. Raman spectra of were recorded with a FI532WH Finder Insight Raman spectrometer (Zolix Instruments Co. Ltd) with 532 nm laser excitation. The contact angle was measured by static contact angle goniometer (JC2000D2M). The surface zeta potential (1 mM KCl solution pH =

5.5 ± 0.2) was measured by a zeta potential analyzer (Surpass). The XRD analysis was performed on a D/MAX-2500 instrument with Cu-Kα radiation. GISAXS measurements were conducted on a Rigaku Smart Lab instrument with an incidence angle of 0.5°.

Electrochemical Measurements

Sulfur electrodes were fabricated by pasting sulfur slurry containing 80 wt% S/CNT composite, 10 wt% carbon black and 10 wt% polyvinylidene fluoride (PVDF) binder onto aluminum foil current collector. The S/CNT composite was prepared by mixing sublimate sulfur and CNT with a mass ratio of 7:3 and heated at 155 °C for 12 h in a sealed tube. The mass loading of active sulfur was around 1.5 mg cm^{-2}. The high sulfur loading electrode was fabricated by 86% S/KB, 5% carbon black, 5% CNT and 4% polyacrylate binder on carbon coated aluminum foil. The sulfur content of S/KB is around 75 %. 30 μL of 1 mol L^{-1} LiTFSI and 1 wt% $LiNO_3$ additive in DME and DOL (1:1 by volume) was used as electrolyte. The Celgard separator is a PP/PE/PP three-layer structure. The CR2032 coin cell was assembled in an argon-filled glove box, and the lithium metal was used as the anode. The galvanostatic charge/discharge performance was investigated using a LAND battery instrument between 1.7 and 2.8 V. The cyclic voltametry (CV) and electrochemical impedance spectroscopy (EIS) measurements were performed on CHI660E electrochemical workstation. CV was performed in a potential window of 1.7-2.8 V (vs. Li^+/Li) at 0.1 mV s^{-1}. EIS was conducted in the frequency range from 0.01 to 10^5 Hz.

Preparation of Li_2S_8

The Li_2S_8 solution (0.3 mol L^{-1}) was prepared by adding S_8 and Li_2S (7:8 molar ratio) in the solvent of DOL and DME (1:1 volume ratio) with a long-term stir at 60 ^oC in an Ar-filled glovebox.

Ionic Conductivity Measurement

The ionic conductivity was measured using the EIS (0.1-100 KHz) by sandwiching the TpPa-SO_3Li/Celgard, TpPa-SO_3H/Celgard or Celgard separators between two stainless steel electrodes according to the following equation:[2]

$$\sigma = L/(R_b \times A)$$

where σ is the ionic conductivity (S cm^{-1}), L stands for the thickness of the membrane (cm), R_b represents the bulk resistance (Ω) and A is the area of the stainless steel electrode (cm^2).

Lithium ion Transference Number Measurement

The lithium ion transference number was measured by sandwiching the TpPa-SO_3Li/Celgard, TpPa-SO_3H/Celgard or Celgard separators, respectively, between two lithium metal electrodes using electrochemical working station (CHI660E). The constant step potential was 10 mV and the lithium ion transference number was defined as the ratio of steady state current to initial state current according to the following equation:[3,4]

$$t_{Li^+} = I_s/I_o$$

where t_{Li^+} is the lithium ion transference number, I_s and I_o represent the current at the steady state and initial state, respectively.

DFT calculations

The transition state search is carried out using Dmol3 package by linear and quadratic synchronous transit (LST/QST) methods. Generalized gradient approximation with Perdew–Burke–Ernzerhof functional (GGA–PBE) was used for the exchange correlation energy. The energy tolerance in the self-consistent field (SCF) calculations was 2×10^{-5} Ha.

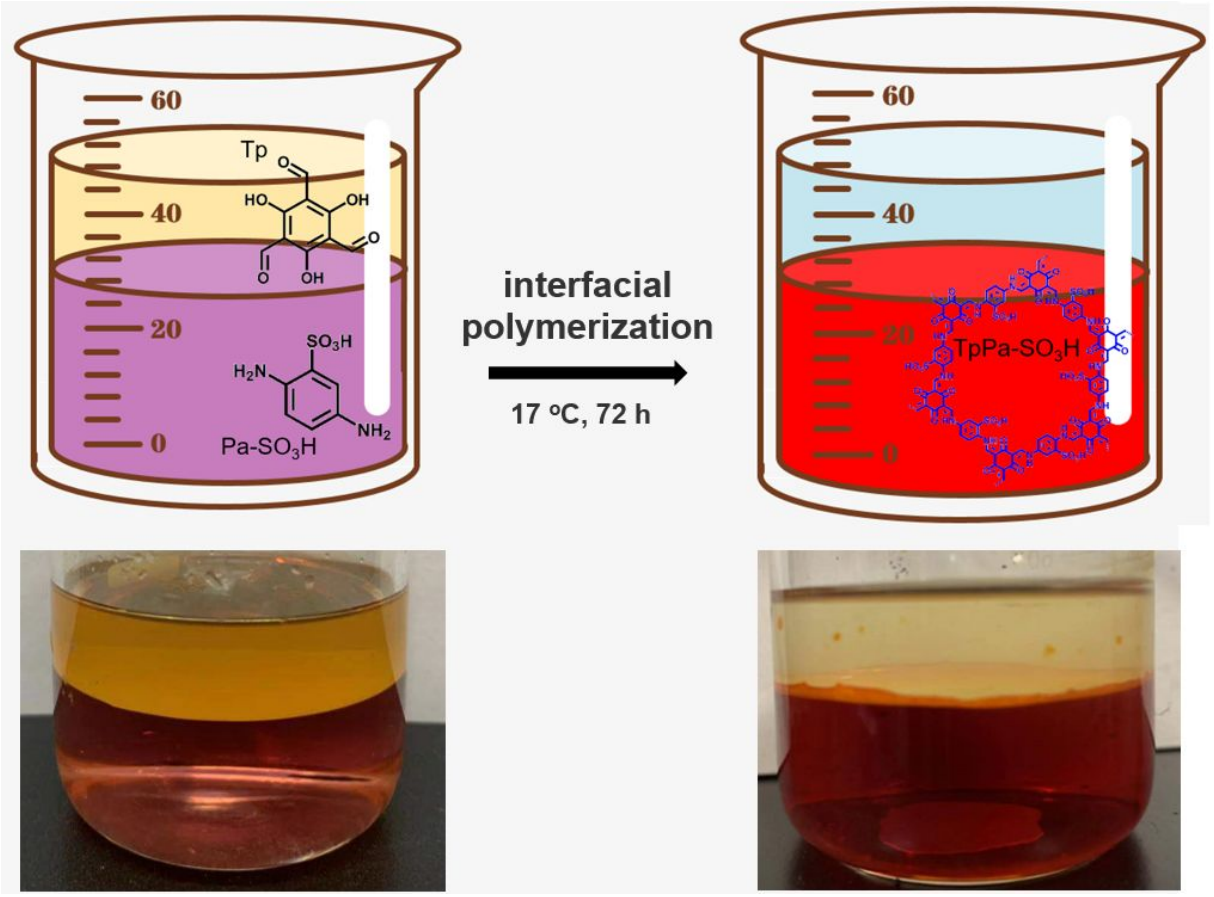

Figure S1. Synthetic scheme of the TpPa-SO_3H nanosheets.

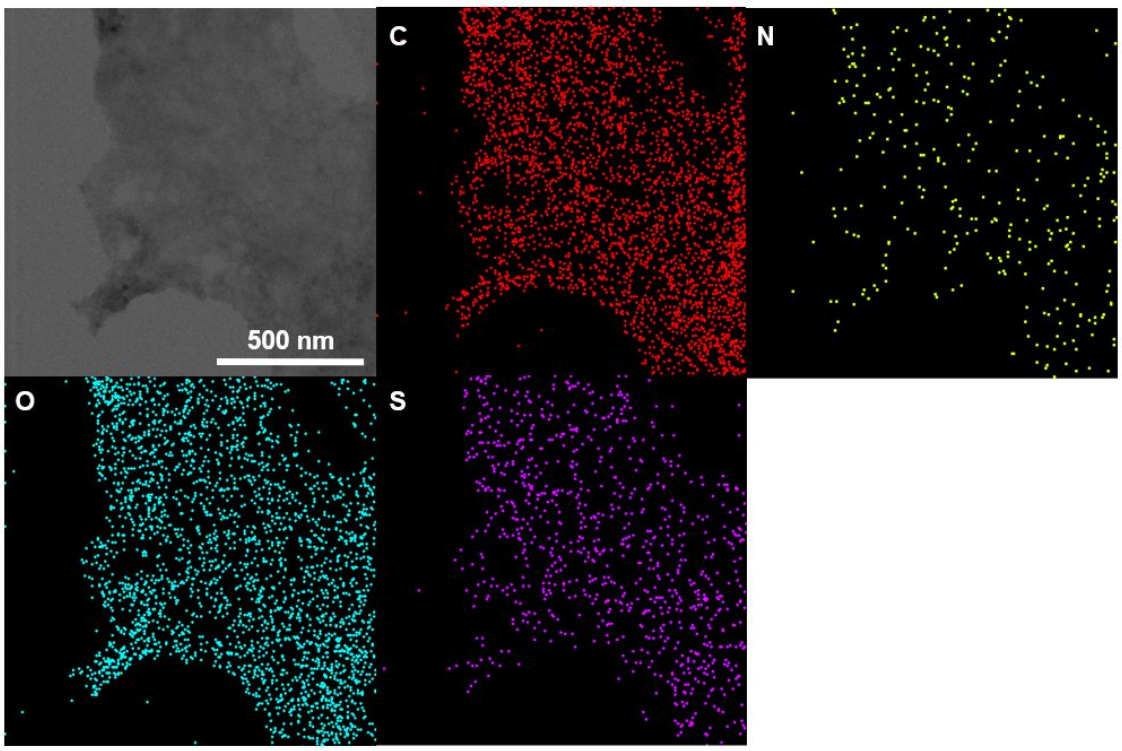

Figure S2. TEM image of the TpPa-SO_3Li nanosheets and corresponding EDS mappings of C, N, O and S elements, respectively.

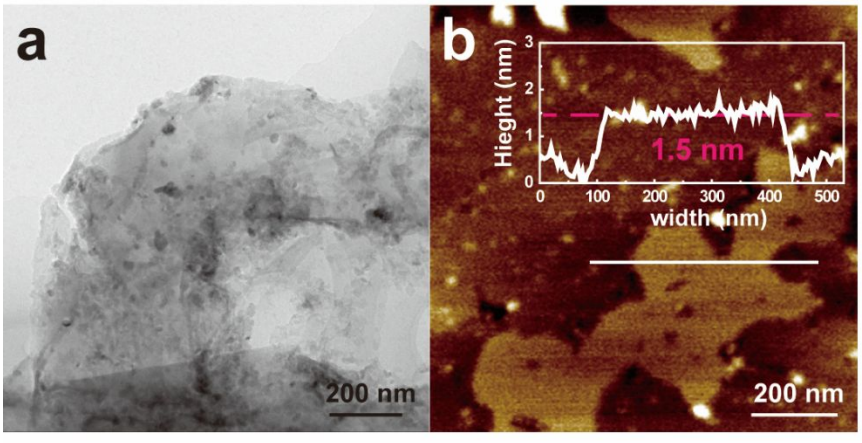

Figure S3. (a) TEM and (b) AFM images of the TpPa-SO_3H nanosheets.

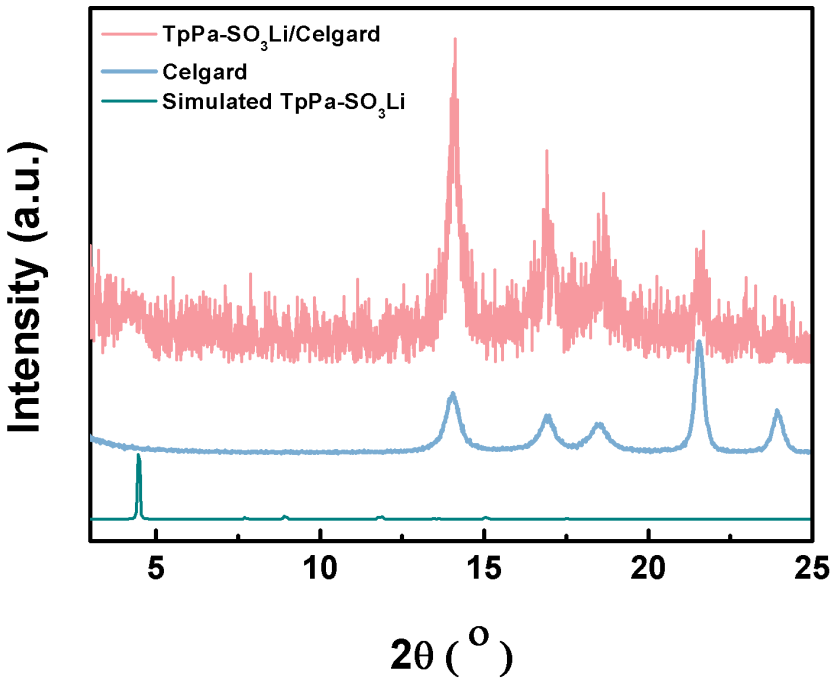

Figure S4. GISAXS spectrum of the TpPa-SO_3Li/Celgard and Celgard separator.

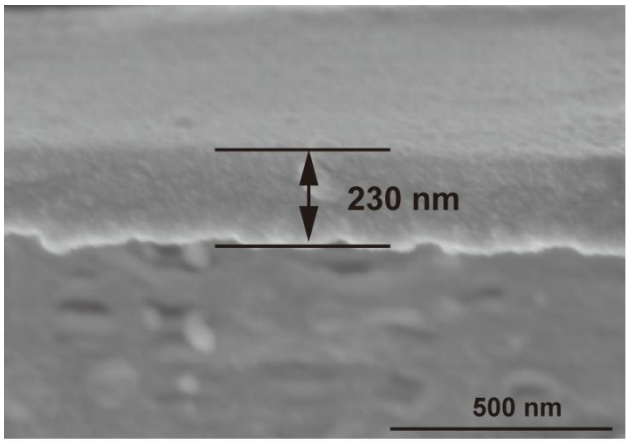

Figure S5. Cross-sectional SEM image of the TpPa-SO_3Li/Celgard separator.

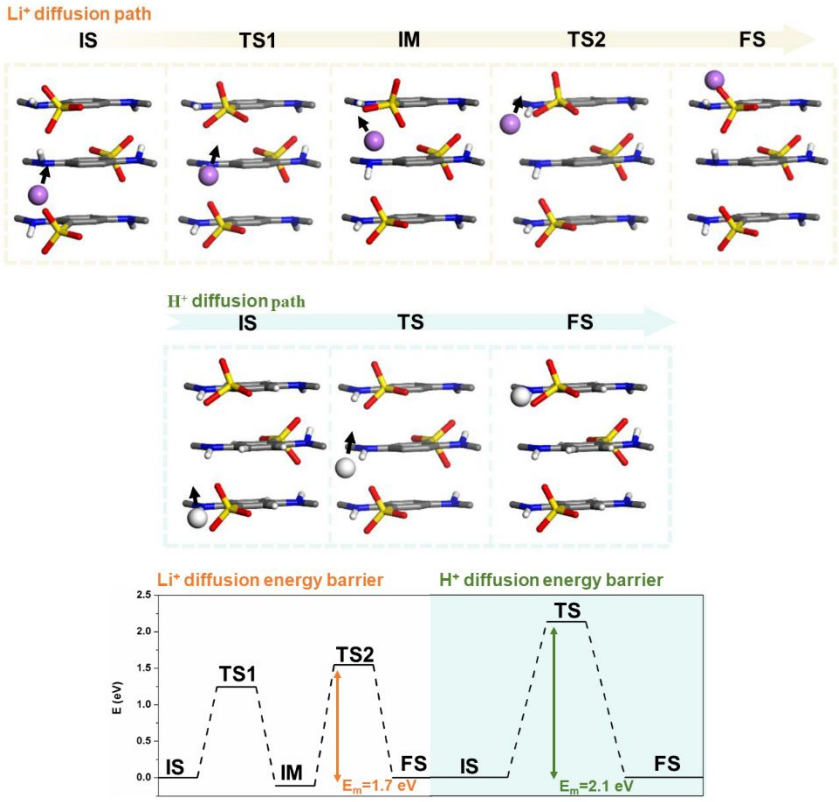

Figure S6. Schematics of Li^+/H^+ diffusion path in the TpPa-SO_3Li/TpPa-SO_3H and the corresponding diffusion energy barrier.

TpPa-SO_3H+LiTFSI→TpPa-SO_3Li+HTFSI (ΔE= -14 eV)……Equation S1

The density functional theory (DFT) caculations were further used to explore the different Li^+ or H^+ conduction properties between the TpPa-SO_3Li and TpPa-SO_3H. As shown in Figure S6, the calculated Li-ion diffusion energy barrier of the TpPa-SO_3Li (1.7 eV) is obviously smaller than that of the TpPa-SO_3H (2.1 eV), indicating a better ionic conduction capability of the TpPa-SO_3Li.

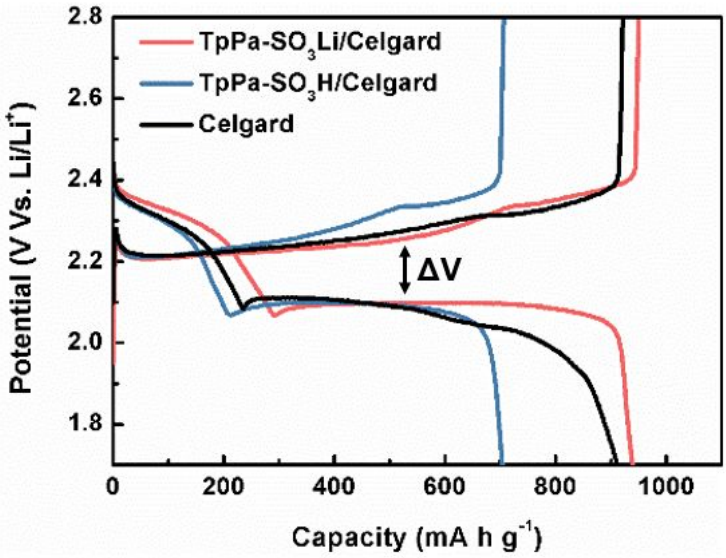

Figure S7. Galvanostatic discharge-charge curves of the Li-S batteries with the TpPa-SO_3Li/Celgard, TpPa-SO_3H/Celgard and Celgard separator at 0.1 C.

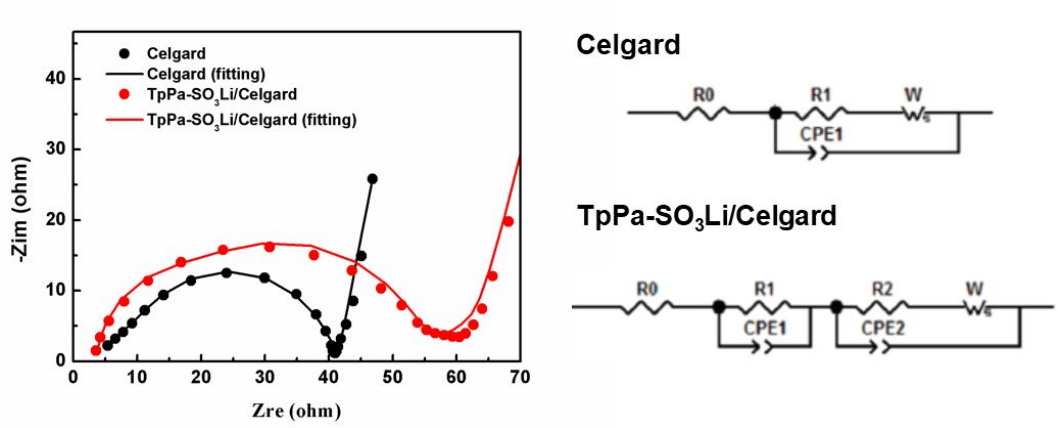

Figure S8. EIS of TpPa-SO_3Li/Celgard cell and pristine Cell and the corresponding equivalent circuits.

The cell using the conventional Celgard separator has only one semicircle, whereas the cell using the TpPa-SO_3Li/Celgard separator has another small semicircle at middle frequency region. Their equivalent circuits indicate that both

of them have charge transfer resistance at sulfur cathode (R1), while the TpPa-SO_3Li/Celgard cell has an interface contact resistance between TpPa-SO_3Li layer and cathode electrode (R2) resulting in the second semicircle.

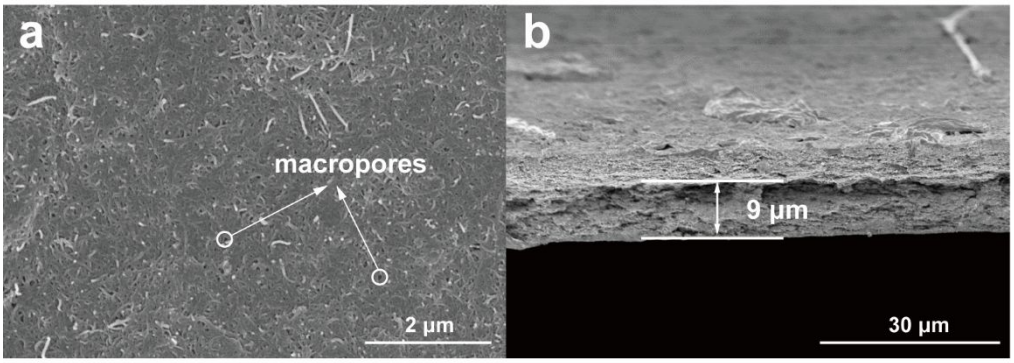

Figure S9. SEM image of the (a) surface and (b) cross-section of the CNT interlayer.

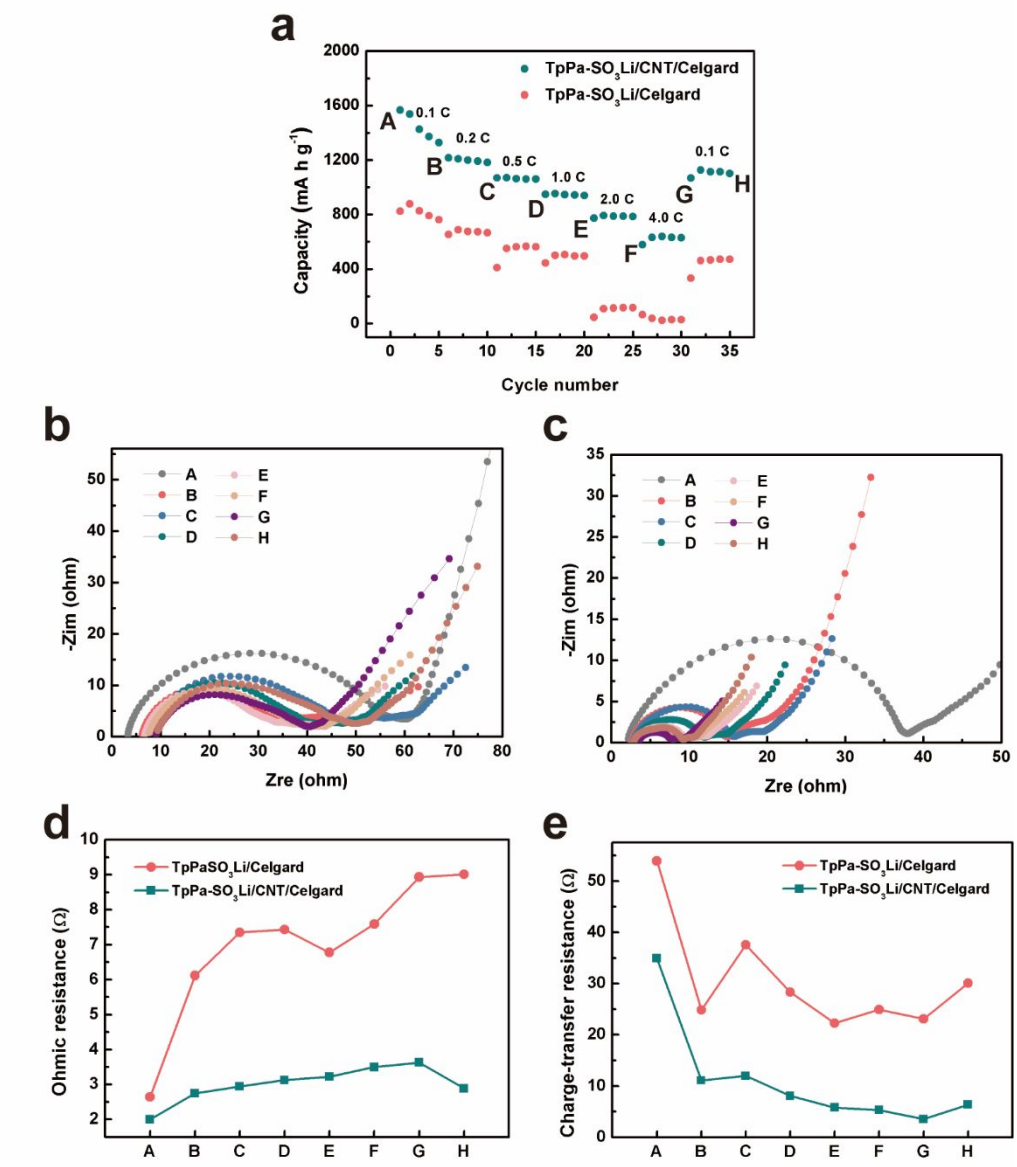

Figure S10. (a) Rate performance of the TpPa-SO_3Li/CNT/Celgard and TpPa-SO_3Li/Celgard cell. EIS of (b) TpPa-SO_3Li/Celgard and (c) TpPa-SO_3Li/CNT/Celgard cell corresponding to different points (A-H) at (a). (d) Ohmic resistance and (e) Charge-transfer resistance of the TpPa-SO_3Li/CNT/Celgard and TpPa-SO_3Li/Celgard cell.

The effect of CNT interlayer was further investigated by EIS at different C rates (Figure S8). The ohmic resistance reflects the internal resistance of the battery, and the charge-transfer resistance represents the difficulty of charge transfer at the interface of cathode. As shown in Figure S8d, the ohmic resistance of the TpPa-SO_3Li/Celgard cell increases significantly with the increase of current density indicating the formation of inert layer. However, the ohmic resistance of the TpPa-SO_3Li/CNT/Celgard cell maintains at a low level at different current density proving the activation effect of the CNT interlayer.

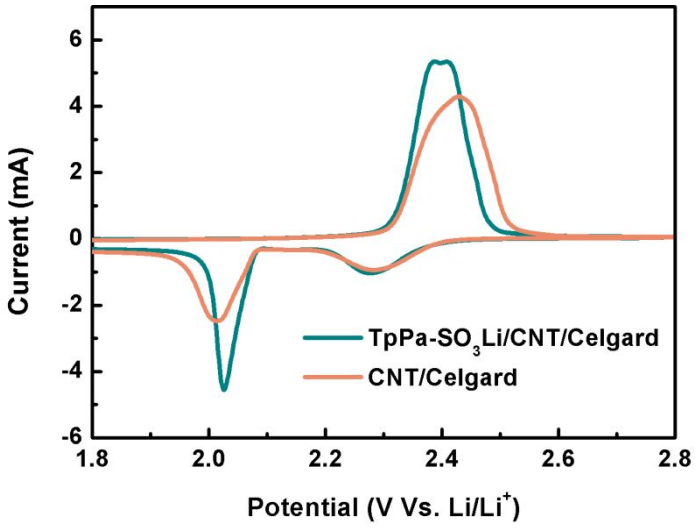

Figure S11. CV curves of the TpPa-SO_3Li/CNT/Celgard and CNT/Celgard cell.

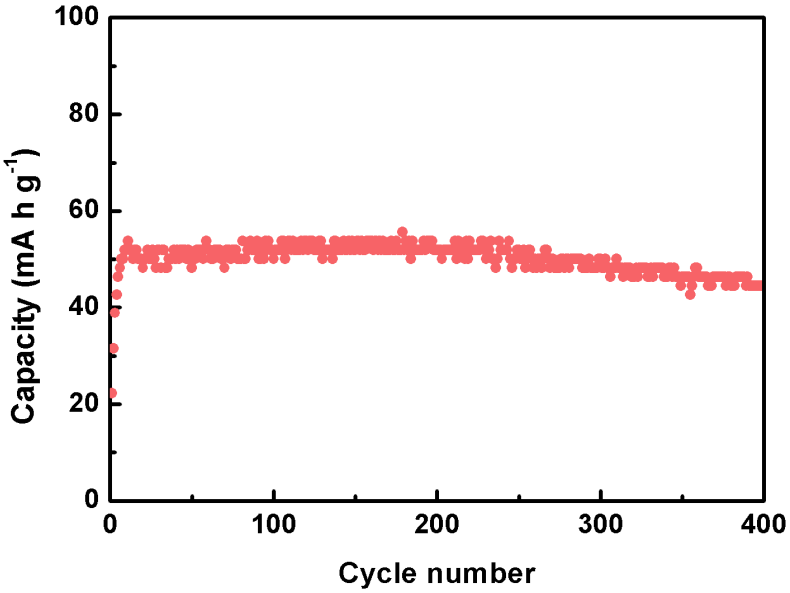

Figure S12. Cycling performance of the TpPa-SO_3Li/Celgard cell at 4.0 C.

Table S1. Parameters for the ionic conductivity calculation of Celgard, TpPa-SO_3H/Celgard and TpPa-SO_3Li/Celgard separator.

Separator	Thickness (μm)	Bulk resistance (Ω)	Area (cm^2)	Ionic conductivity (mS cm^{-1})
Celgard	33±0.3	1.73	2	0.95
TpPa-SO_3H/Celgard	33±0.3	3.17	2	0.52
TpPa-SO_3Li/Celgard	33±0.3	2.64	2	0.62

Table S2. Electrochemical performance of various modified separators based on COFs or Li-ion selective transport mechanism in Li-S batteries.

Modified layer	Layer thickness (μm)	S loading (mg cm^{-2})	Li-ion transference number	Cycle performance	Fading rate per cycle (%)	Reference
MoS_2	0.35		0.62	401 mA h g^{-1} (0.5 C, 600 cycles)	0.083	3
GO			0.21	308 mA h g^{-1} (0.5 C, 350 cycles)	0.182	3
COF-1	28	1.0-1.5		~600 mA h g^{-1} (1 C, 250 cycles)	0.182	5
TP-BPY-COF	~3	1-1.5		826 mA h g^{-1} (1 C, 250 cycles)	0.173	6
Li-CON@GN	5	1-2	0.82	645 mA h g^{-1} (1 C, 600 cycles)	0.057	7
DMTA-COF		1.5		457 mA h g^{-1} (2 C, 500 cycles)	\	8
DMTA-COF@CNT		2		658 mA h g^{-1} (~1.2 C, 700 cycles)	0.070	9
DMTA-COF@CN		10		731 mA h g^{-1} (0.06 C, 60 cycles)	0.317	9
TpPa-SO_3Li	0.23	5.4	0.88	639 mA h g^{-1} (0.2 C, 100 cycles)	0.224	This work
TpPa-SO_3Li with CNT interlayer	0.23	1.5		482 mA h g^{-1} (4 C, 400 cycles)	0.039	This work

References

(1) Cao, L.; Wu, H.; Cao, Y.; Fan, C.; Zhao, R.; He, X.; Yang, P.; Shi, B.; You, X.; Jiang, Z. Weakly Humidity-Dependent Proton-Conducting COF Membranes. *Adv. M*ater. **2020,** 2005565.

(2) Yang, Y.; Zhang, J. Highly Stable Lithium–Sulfur Batteries Based on Laponite Nanosheet–Coated Celgard Separators. *Adv. Energy Mater.* **2018,** *8*, 1801778.

(3) Ghazi, Z. A.; He, X.; Khattak, A. M.; Khan, N. A.; Liang, B.; Iqbal, A.; Wang, J.; Sin, H.; Li, L.; Tang, Z. MoS_2/Celgard Separator as Efficient Polysulfide Barrier for Long-Life Lithium–Sulfur Batteries. *Adv. Mater.* **2017,** *29*, 1606817.

(4) Bruce, P. G.; Evans, J.; Vincent, C. A. Conductivity and transference number measurements on polymer electrolytes. *Solid State Ionics.* **1988,** *28-30*, 918-922.

(5) Jiang, C.; Tang, M.; Zhu, S.; Zhang, J.; Wu, Y.; Chen, Y.; Xia, C.; Wang, C.; Hu, W. Constructing Universal Ionic Sieves via Alignment of Two-Dimensional Covalent Organic Frameworks (COFs). *Angew. Chem. Int. Ed.* **2018,** *57*, 16072-16076.

(6) Xu, Q.; Zhang, K.; Qian, J.; Guo, Y.; Song, X.; Pan, H.; Wang, D.; Li, X. Boosting Lithium–Sulfur Battery Performance by Integrating a Redox-Active Covalent Organic Framework in the Separator. *ACS Appl. Energy Mater.* **2019,** *2*, 5793-5798.

(7) Cao, Y.; Liu, C.; Wang, M.; Yang, H.; Liu, S.; Wang, H.; Yang, Z.; Pan, F.; Jiang, Z.; Sun, J. Lithiation of covalent organic framework nanosheets facilitating lithium-ion transport in lithium-sulfur batteries. *Energy Storage Mater.* **2020,** *29*, 207-215.

(8) Wang, J.; Si, L.; Wei, Q.; Hong, X.; Cai, S.; Cai, Y. Covalent Organic Frameworks as the Coating Layer of Ceramic Separator for High-Efficiency Lithium–Sulfur Batteries. *ACS Appl. Nano Mater.* **2018,** *1*, 132-138.

(9) Wang, J.; Qin, W.; Zhu, X.; Teng, Y. Covalent organic frameworks (COF)/CNT nanocomposite for high performance and wide operating temperature lithium-sulfur batteries. *Energy* **2020,** *199*, 117372.